Burns 52 (2026) 107944

Contents lists available at ScienceDirect

Burns

journal homepage: www.elsevier.com/locate/burns

Quantitative assessment of lung microstructure and functional changes of smoke-inhalation-induced acute lung injury with hyperpolarized ^{129}Xe magnetic resonance

Shuguang Xie [a,c,1], Haidong Li [b,d,1], Yu Zheng [b,1], Wenjie Wang [b,d], Ming Zhang [b,d], Hongchuang Li [b,d], Xiuchao Zhao [b,d], Lianjie Li [c], Li Fan [c], Yi Xiao [c], Yeqing Han [b,d], Shiyuan Liu [a,c,*], Xin Zhou [b,d,e,**]

[a] School of Medical Imaging, Xuzhou Medical University, Xuzhou, Jiangsu 221000, China
[b] State Key Laboratory of Magnetic Resonance Spectroscopy and Imaging, National Center for Magnetic Resonance in Wuhan, Innovation Academy for Precision Measurement Science and Technology, Chinese Academy of Sciences-Wuhan National Laboratory for Optoelectronics, Huazhong University of Science and Technology, Wuhan, Hubei 430071, China
[c] Department of Radiology, Second Affiliated Hospital of Naval Medical University, Shanghai 200003, China
[d] University of Chinese Academy of Sciences, Beijing 100049, China
[e] School of Biomedical Engineering, Hainan University, Haikou 570228, China

ARTICLE INFO

Keywords:
Smoke inhalation injury
Gas exchange, hyperpolarized ^{129}Xe, acute lung injury

ABSTRACT

Background: Accurate assessment of smoke-inhalation-induced acute lung injury (SI-ALI) is essential for clinical diagnosis and effective management. Hyperpolarized ^{129}Xe magnetic resonance (MR), an emerging imaging modality, has shown broad utility across various pulmonary conditions. This study aimed to evaluate the feasibility and potential of hyperpolarized ^{129}Xe MR for assessing gas exchange impairment and microstructural alterations in the lungs following SI-ALI.

Method: Two groups of rats (n = 5 per group) were studied. The smoke inhalation injury (SII) group was subjected to three 2-minute exposures to pine sawdust smoke under general anesthesia with endotracheal intubation. The sham group underwent identical procedures but was exposed to clean air. Twenty-four hours after exposure, pulmonary function tests, micro-computed tomography (micro-CT), and ^{129}Xe MR examinations were conducted to obtain quantitative physiological parameters. Subsequently, lung tissues were harvested for histological analysis of alveolar septal wall thickness.

Result: Rats exposed to smoke (SII group) showed significant decreases in lung volume, as indicated by reduced total lung capacity (TLC, $p = 0.036$) and forced vital capacity (FVC, $p = 0.020$). They also had signs of airway obstruction, with lower forced expiratory volume in 100 ms (FEV_{100}, $p = 0.041$) and maximal mid-expiratory flow (MMEF, $p = 0.014$). Hyperpolarized ^{129}Xe MR spectroscopy showed a lower red blood cell to tissue/plasma (RBC/TP) signal ratio in the SII group (0.45 ± 0.04) compared to the sham group (0.51 ± 0.04, $p = 0.035$), suggesting impaired gas exchange. The gas exchange time constant increased from 21.22 ms to 28.86 ms ($p = 0.013$), and the septal wall thickness measured by MR also increased (from 8.28 μm to 9.68 μm, $p = 0.013$). These MR results matched well with histological measurements, which also showed thickened alveolar walls (from 6.99 μm to 7.70 μm). Ventilation imaging revealed clear areas of reduced airflow, which corresponded to regions of lung consolidation seen on micro-CT scans.

Conclusion: Hyperpolarized ^{129}Xe MR enables quantitative evaluation of both functional and microstructural lung changes in a rat model of SI-ALI. These findings highlight its potential as a powerful noninvasive tool for assessing smoke-inhalation-induced acute lung injury.

* Correspondence to: No. 415 Fengyang Road, Shanghai 200003, China.
** Correspondence to: No. 30 Xiaohong West, Wuchang, Wuhan 430071, China.
E-mail addresses: cjr.liushiyuan@vip.163.com (S. Liu), xinzhou@wipm.ac.cn (X. Zhou).
[1] Shuguang Xie, Haidong Li and Yu Zheng contributed equally to this work

https://doi.org/10.1016/j.burns.2026.107944
Accepted 26 February 2026
Available online 27 February 2026

1. Introduction

Smoke-inhalation-induced acute lung injury (SI-ALI) refers to damage to the respiratory tract and lung parenchyma caused by the inhalation of irritating smoke, toxic gases, and heat. It is a common and serious complication among burn patients. The smoke generated during combustion contains a complex mixture of toxic substances and fine particles that can directly injure the airways and lung tissue. These injuries can lead to airway obstruction, reduced bronchial clearance, and the accumulation of local inflammatory mediators, manifesting clinically as coughing, wheezing, dyspnea, and, in severe cases, respiratory failure or asphyxiation [1]. Epidemiologically, SI-ALI is an independent risk factor for mortality, increasing the risk by approximately 20%. When combined with pneumonia, this risk rises to nearly 60% [2]. Moreover, SI-ALI is strongly associated with prolonged hospital stays and elevated in-hospital mortality rates [3,4]. Given its significant clinical impact, prompt and accurate diagnosis is critical for optimizing treatment strategies and improving patient outcomes.

However, current clinical diagnostic methods have notable limitations. Although conventional chest radiography and computed tomography (CT) are effective for visualizing structural abnormalities, they lack the capacity to evaluate pulmonary ventilation or gas exchange functions in SI-ALI. These functional disturbances represent key aspects of disease severity and progression, yet remain inaccessible to morphology-based imaging techniques [5,6]. Fiberoptic bronchoscopy (FOB) allows for direct visualization and lavage of the bronchial tree [7], and it plays a role in injury grading via the Abbreviated Injury Score (AIS) and determining the extent of SI-ALI [8]. Nonetheless, FOB is limited in its ability to detect injuries in the distal airways, respiratory bronchioles, and alveoli, which constrains its predictive value for severe outcomes such as acute respiratory distress syndrome (ARDS) [9]. Other examination methods, such as arterial blood gas analysis and the measurement of inflammatory markers (e.g., IL-1Ra, IL-6, IL-8), have shown correlations with prognosis. However, their utility for early and specific diagnosis remains uncertain and requires further validation [10]. These limitations highlight the need for new, non-invasive techniques capable of providing both structural and functional insights into SI-ALI.

Hyperpolarized ^{129}Xe magnetic resonance imaging (HP ^{129}Xe MRI) is an emerging, non-invasive, radiation-free imaging modality that enables direct visualization and quantitative evaluation of pulmonary ventilation and gas exchange [11]. This technique has been approved for clinical use and has demonstrated significant value in assessing various respiratory disorders, including chronic obstructive pulmonary disease (COPD), pulmonary fibrosis, and asthma [12–16]. HP ^{129}Xe MRI allows for the assessment of both lung microstructural and functional changes, offering a comprehensive view of respiratory pathophysiology. Despite its promise, its application in SI-ALI has not been systematically explored.

In this study, we established a rat model of SI-ALI and utilized HP ^{129}Xe MRI to evaluate both structural and functional changes in the lung. We compared our imaging findings with pulmonary function tests (PFTs), micro-CT, and histopathological analysis to assess the diagnostic potential of HP ^{129}Xe MR.

2. Materials and methods

2.1. Animal preparation

All animal experimental protocols were approved by the Institutional Review Board. Ten male Sprague-Dawley rats (body weight: 300–400 g) were acclimatized for 7 days with free access to standard laboratory chow and water. The rats were randomly divided into two groups: the smoke-inhalation-injury (SII) and the sham groups (n = 5 per group).

All the examinations were performed 24 h after smoke exposure. Animals were anaesthetized via intraperitoneal injection of sodium pentobarbital (45 mg/kg) and subsequently intubated with 14-gauge endotracheal catheters. Each rat underwent a sequential experimental protocol consisting of pulmonary function tests (PFTs), hyperpolarized ^{129}Xe MR examinations, Micro-CT scanning, and terminal lung tissue collection.

2.2. Smoke inhalation injury

The SI-ALI model was established following previously reported procedures [17]. Smoke was generated by smoldering 30 g of pine sawdust in a 500 mL flask heated to 400°C on a hotplate (Fig. 1 A). To prevent condensation, a desiccant-containing flask was inserted between the smoke source and inhalation chamber (45 × 20 × 20 cm^3). Smoke density was standardized to 20–30% on the Ringelmann chart by adjusting the airflow through a dual-pump system, achieving chamber saturation within 30 s. Each rat in SII group received three 2-minute exposures to smoke (totaling 6 min of cumulative smoke inhalation), with 1-minute recovery intervals between exposures (Fig. 1B). Successful exposure was confirmed visually by the presence of soot deposition on the endotracheal tubes. The sham group underwent identical handling procedures but was exposed to clean air.

2.3. Pulmonary function tests

Pulmonary function tests (PFTs) were performed on anesthetized and tracheostomized rats using a commercial forced maneuvers system (CRFM 100, EMMS, Bordon, UK). Following baseline correction, the system inflated the lungs to 30 cmH_2O and briefly maintained this pressure before initiating a forced expiration by connecting the airway to a negative pressure reservoir. Expiration continued until the respiratory flow reached zero, with the expiratory rate limited by the animal's pulmonary resistance. Forced vital capacity (FVC) was defined as the total volume of air exhaled completely and forcefully after maximal inspiration. In addition, total lung capacity (TLC), forced expiratory volume in 100 ms (FEV_{100}), and maximal mid-expiratory flow (MMEF) were also measured. All PFTs examinations were completed within 5 min.

2.4. ^{129}Xe polarization and delivery

Isotopically enriched xenon gas (86% ^{129}Xe) was polarized by spin-exchange optical pumping using a commercial polarizer system (VIP 510, verImagin Healthcare; Wuhan, China) operating in continuous-flow mode. A total of 120 mL of hyperpolarized ^{129}Xe gas was cryogenically collected and subsequently thawed into a Tedlar bag. The available spin polarization was approximately 40%.

2.5. ^{129}Xe MR examinations

Following PFTs, MR examinations were performed on all the rats using a 7 T animal MRI (Bruker Biospec 70/20 USR, Billerica, MA, USA) equipped with a home-built ^{129}Xe birdcage coil. During MR experiments, rats were maintained under anesthesia with 1% isoflurane, positioned supine, and alternately ventilated with hyperpolarized ^{129}Xe and oxygen gas via a custom-built gas delivery system with real-time airway pressure monitoring and MR acquisition triggering. Each rat underwent ^{129}Xe ventilation imaging and magnetic resonance spectroscopy (MRS) to assess pulmonary ventilation and gas-blood exchange function.

For hyperpolarized ^{129}Xe ventilation imaging, rats were flushed three times with xenon gas to enhance signal-to-noise ratio (SNR). Imaging was performed during a single breath-hold using a 2D gradient-echo sequence with the following parameters: repetition time (TR) = 7.6 ms; echo time (TE) = 2.2 ms; number of slices = 7; slice thickness = 4 mm; matrix = 96 × 96; field of view (FOV) = 50 mm × 50 mm; flip angle = 10°; and bandwidth = 50 kHz [18].

For hyperpolarized ^{129}Xe MRS, chemical shift saturation recovery

(CSSR) was performed as previously described [19]. Two Gaussian pulses (0.5 ms and 0.3 ms) were used to selectively saturate and excite dissolved ^{129}Xe signals, minimizing off-resonance effects on gas-phase ^{129}Xe (0.05° and 0.13°, respectively). Spectra were acquired with a 25 kHz bandwidth and 1024 sampling points across 24 exchange times ranging from 2 to 400 ms. To improve SNR, each spectrum was acquired five times during a single 4-second xenon gas breath-hold following two xenon flushes.

2.6. ^{129}Xe MR Data processing

All MR data were analyzed using MATLAB software (The MathWorks, Inc., Natick, MA). For hyperpolarized ^{129}Xe gas exchange, spectral data were fitted to the Lorentzian curves to extract ^{129}Xe signal amplitudes for tissue and plasma (TP), red blood cells (RBC), and gas phase components. TP and RBC signal were normalized to the gas-phase signal and further analyzed using the model of gas exchange for hyperpolarized ^{129}Xe in the lung (MOXE) to quantify pulmonary physiological parameters, including exchange time constant (T), septal wall thickness (d), and dissolved surface area to gas volume ratio (SVR) [20,21]. In addition, ratios of RBC/Gas, TP/Gas, and RBC/TP were calculated using the spectra obtained at an exchange time of 100 ms.

2.7. Micro-CT scans

Following the MR examinations, all rats underwent CT scans using a Micro-CT system (SkyScan1176, Bruker, Kontich, Belgium). During imaging, ventilation was regulated via a custom-built gas delivery system, maintaining a tidal volume of 2.5 mL. Image acquisition was synchronized with the end-inspiratory phase to ensure consistency and accuracy. Scanning parameters were set as follows: source voltage = 80 kV, source current = 313 μA, spatial resolution = 35 μm × 35 μm, exposure time = 75 ms, rotation steps = 0.7° and filter selected aluminum 1 mm. Image reconstruction was carried out using NRecon software (v1.7.4.6, SkyScan) with the following parameters: Gaussian smoothing (kernel = 2, smoothing = 6), ring artifact correction = 10, and 30% beam hardening correction. Image post-processing was conducted using ITK-SNAP software (v4.0.2) [22] to extract mean lung density (MLD) as a quantitative CT parameter.

2.8. Tissue harvesting and quantitative histology

Following micro-CT imaging, rats were euthanized and lung tissues were harvested. The lungs were inflated with 4% paraformaldehyde at a constant pressure of 25 cm H_2O and immersion-fixed in the same solution for at least 48 h. To ensure consistency and comparability, histological samples were harvested from every lobe of each lung. The tissues were then embedded in paraffin, cut into 5μm-thick sections (yielding a total of six sections per rat), and stained with hematoxylin and eosin (H&E) for histological evaluation. For each section, three representative images that excluded major airways were acquired using a Nikon Eclipse Ts 100 microscope (Nikon Corporation, Tokyo, Japan). A standard test grid was overlaid on the images to determine alveolar septal wall thickness as the mean truncated length [23]. Images were analyzed using Image-Pro Plus software (Media Cybernetics, Buckinghamshire, UK) to calculate the wall septal wall thickness [24,25].

2.9. Statistical analysis

SPSS software (version 27.0, IBM Inc., Chicago, IL, USA) was used for statistical analysis. Differences between the SII and sham groups were assessed using unpaired two-tailed *t*-tests. Correlations between parameters were evaluated using Spearman's correlation analysis. A *p*-value < 0.05 was considered statistically significant for all tests.

3. Results

3.1. Pulmonary function tests

PFTs revealed significant impairments in the SII group compared to sham controls (Table 1). Rats in the SII group exhibited marked reductions in FVC (8.26 ± 1.64 mL vs. 10.44 ± 0.37 mL, $p = 0.020$), TLC

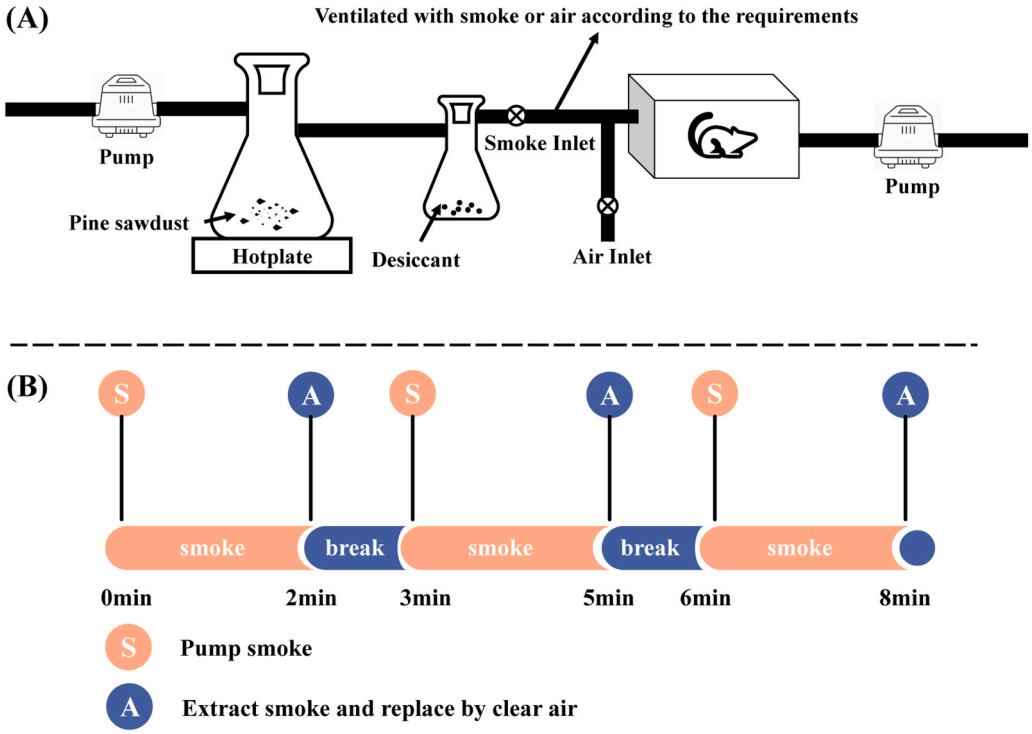

Fig. 1. (A) Schematic diagram of the smoke generation setup. (B) Smoke exposure protocol.

Table 1
Summary of the physiological and morphological parameters measured with PFTs, hyperpolarized ^{129}Xe magnetic resonance.

Parameters	Sham	SII	*p* value
PFTs			
FVC (mL)	10.44 ± 0.37	8.26 ± 1.64	**0.020**[a]
TLC (mL)	11.65 ± 0.42	10.34 ± 1.09	**0.036**[a]
FEV_{100} (mL)	3.81 ± 0.50	2.52 ± 1.07	**0.041**[a]
MMEF (mL/s)	47.45 ± 5.77	25.66 ± 14.45	**0.014**[a]
Gas exchange			
RBC/TP	0.51 ± 0.04	0.45 ± 0.04	**0.035**[a]
RBC/Gas ($\times 10^{-2}$)	1.05 ± 0.20	0.76 ± 0.21	0.059
TP/Gas ($\times 10^{-2}$)	2.03 ± 0.27	1.68 ± 0.33	0.097
d-Xe (μm)	8.28 ± 0.77	9.68 ± 0.61	**0.013**[a]
T (ms)	21.22 ± 3.91	28.86 ± 3.71	**0.013**[a]
SVR (cm^{-1})	345.43 ± 44.46	238.55 ± 43.64	**0.009**[a]

Notes: The *p* values were calculated between the two groups with significant differences in bold.
Abbreviations: FVC, forced vital capacity; TLC, total lung capacity; MMEF, maximal mid expiratory flow; RBC, red blood cells; TP, interstitial tissue/plasma; d-Xe, septal wall thickness derived from ^{129}Xe MRI; T, exchange time constant; SVR, dissolved surface area to gas volume ratio.
[a] Unpaired *t*-test, $p < 0.05$.

(10.34 ± 1.09 mL vs. 11.65 ± 0.42 mL, $p = 0.036$), FEV_{100} (2.52 ± 1.07 mL vs. 3.81 ± 0.5 mL, $p = 0.041$), and MMEF (25.66 ± 14.45 mL/s vs. 47.45 ± 5.77 mL/s, $p = 0.014$). These findings suggest the presence of critical airway obstruction.

3.2. Ventilation function and structure assessment with ^{129}Xe MRI and Micro-CT

Representative ^{129}Xe ventilation images for the sham and SII groups are shown in Fig. 2 A. At 24 h post-smoke exposure, rats in SII group exhibited pronounced ventilation defects and reduced ventilation regions on ^{129}Xe MRI, consistent with micro-CT findings of lung consolidation and ground-glass opacities indicative of acute injury. In contrast, rats in the sham group demonstrated normal ventilation and unremarkable CT findings. Quantitative analysis revealed that mean lung density (MLD) was significantly higher in the SII group (-583 ± 18 HU) compared to the sham group (-633 ± 34 HU, $p = 0.034$).

3.3. Gas exchange function assessment with ^{129}Xe MR

Gas exchange function related parameters extracted using MOXE are summarized in Table 1. Quantitative analysis showed a significant increase in T (28.86 ± 3.71 vs. 21.22 ± 3.91 ms, $p = 0.013$) and d (9.68 ± 0.61 μm vs. 8.28 ± 0.77 μm, $p = 0.013$) in the SII group. Moreover, the measured SVR was significantly reduced in the SII group (238.55 ± 43.64 cm^{-1}) compared to the sham group (345.43 ± 44.46 cm^{-1}, $p = 0.009$).

Fig. 3A shows typical dissolved xenon signal recovery curves from the SII and sham groups. Both the tissue-plasma (TP) and red blood cell (RBC) xenon signals were reduced in the SII group, with a more marked decrease in RBC signal. Mean ratios of RBC/Gas, TP/Gas, and RBC/TP are shown in Fig. 3B , derived from CSSR spectra at an exchange time of 100 ms [25]. The RBC/TP ratio decreased from 0.51 ± 0.04 in the sham group to 0.45 ± 0.04 in the SII group with a statistical significance ($p = 0.035$).

3.4. Quantitative histology

H&E-stained lung sections (Fig. 4 A) showed neutrophil infiltration, alveolar wall thickening, and extensive alveolar edema in the SII group. Quantitative histology analysis revealed an increase in septal wall thickness from 6.99 ± 0.08 μm in the sham group to 7.70 ± 0.17 μm in the SII group ($p < 0.01$). Furthermore, septal wall thickness measured by hyperpolarized ^{129}Xe MR correlated significantly with histological measurements ($R^2 = 0.72$, $p = 0.013$), as shown in Fig. 4B.

4. Discussion

In this study, we demonstrated the feasibility of hyperpolarized ^{129}Xe MR for evaluating pulmonary physiological changes in SI-ALI. We established and evaluated rat models of SI-ALI to quantitatively assess the effects of smoke exposure on pulmonary microstructure and function. Significant differences in pulmonary physiological function between the sham and SII groups were identified using hyperpolarized ^{129}Xe MR, which also showed strong correlations with TLC, FVC, MLD, and histological findings, highlighting its comprehensive assessment capability. These findings indicate hyperpolarized ^{129}Xe MR as a promising tool for clinical evaluation of smoke inhalation injuries.

Toxic particles and gases in smoke initiate inflammatory cascades, damaging the lower respiratory tract and alveoli. This would lead to

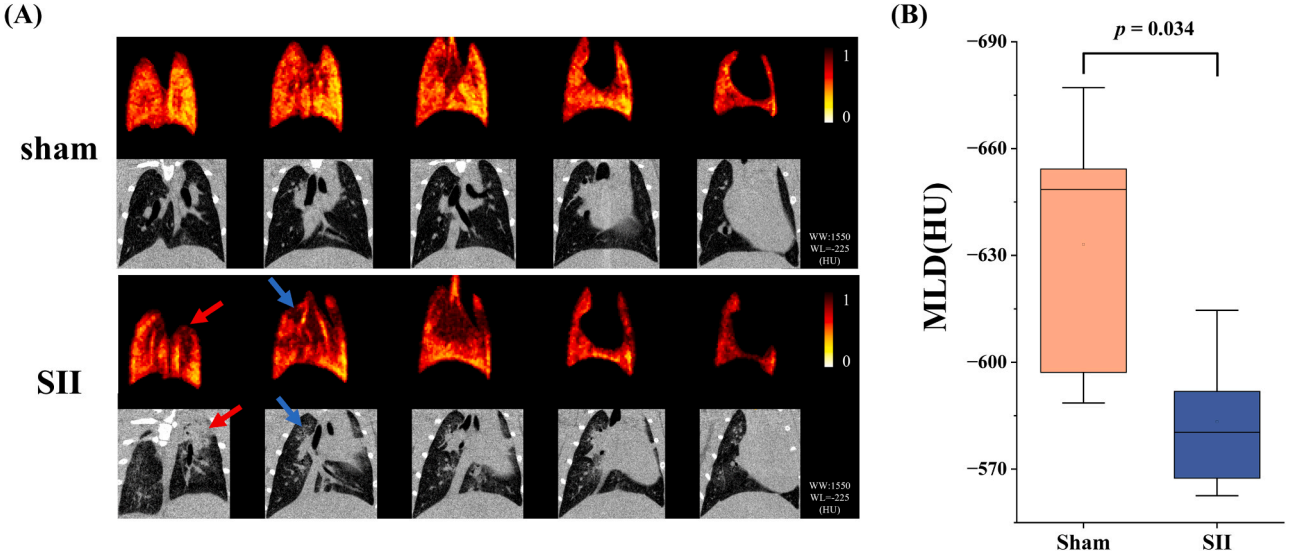

Fig. 2. (A) Hyperpolarized ^{129}Xe ventilation imaging of sham and SII group (top row) and the corresponding Micro-CT slice (bottom row). The blue arrow indicates ground-glass opacification, and the red arrow indicates lung consolidation. (B) MLD comparison between the sham and SII groups.

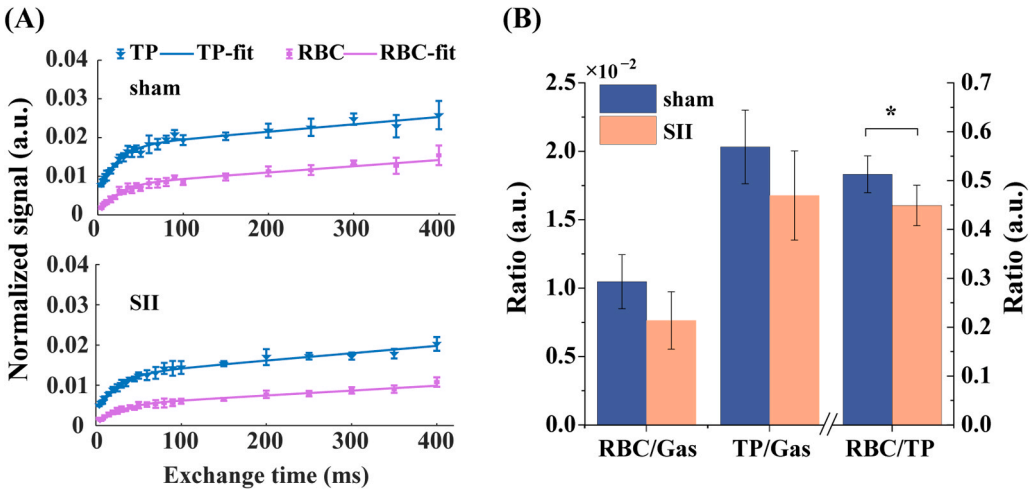

Fig. 3. (A) Representative dissolved xenon signal recovery curves for sham and SII rats. Each data point represents the average of five independent experiments. (B) Comparison of RBC/Gas, TP/Gas, and RBC/TP ratios between the SII and sham groups. A significantly lower RBC/TP ratio was observed in the SII group ($p < 0.05$).

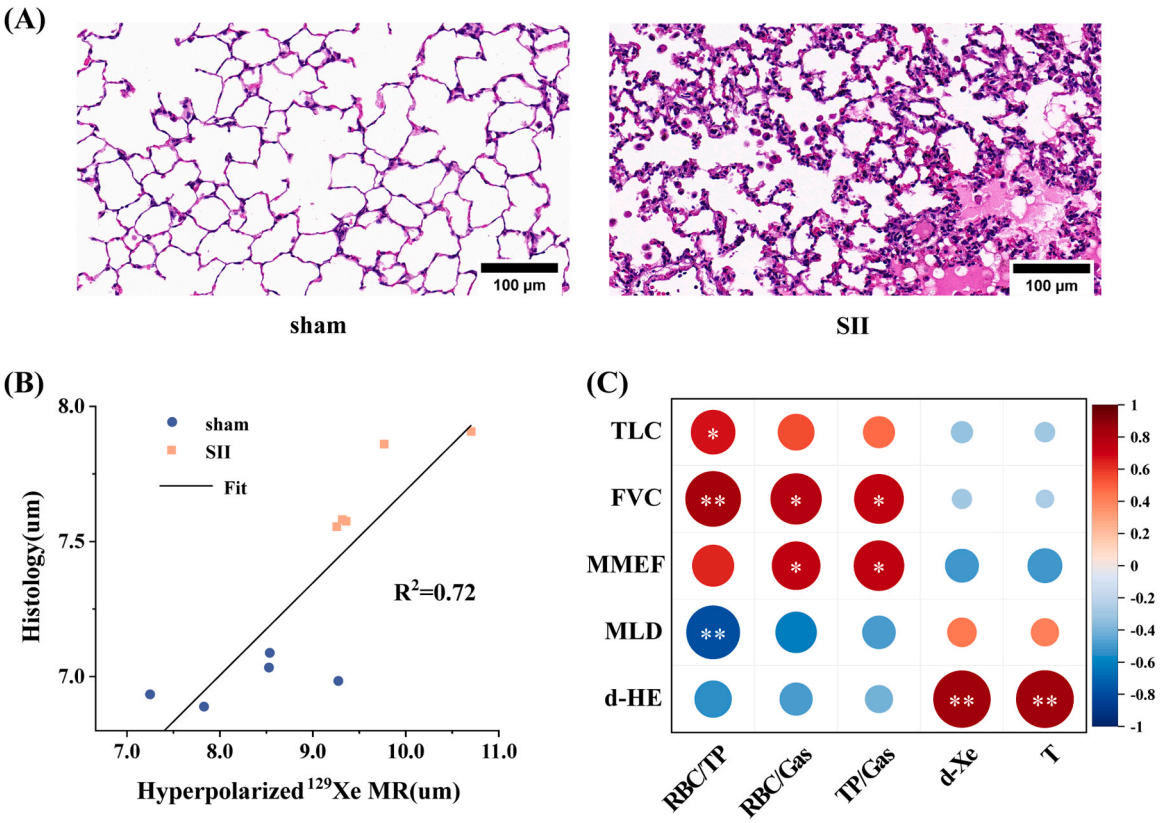

Fig. 4. (A) H&E-stained lung tissue from representative sham and SII rats. The SII group exhibited neutrophil infiltration and alveolar wall thickening, accompanied by extensive edema fluid exudation into the alveolar spaces. (B) Correlation of the septal wall thickness derived from ^{129}Xe gas exchange and quantitative histology. (C) Heatmap illustrating the correlation among PFTs, CSSR, MLD and histological parameters. *$p < 0.05$, **$p < 0.01$. Abbreviations: FVC, forced vital capacity; TLC, total lung capacity; MMEF, maximal mid expiratory flow; RBC, red blood cells; TP, interstitial tissue/plasma; d-Xe, septal wall thickness derived from ^{129}Xe MRI; d-HE, septal wall thickness derived from histology; T, exchange time constant.

bronchoconstriction, exudate formation, and airway obstruction [26–28]. Our results mechanistically link these structural changes to functional impairments. Ventilation defects observed on ^{129}Xe MRI were spatially consistent with high-density areas detected by Micro-CT, demonstrating that hyperpolarized ^{129}Xe MRI effectively reflects ventilation status in SI-ALI.

The RBC/TP ratio exhibited high sensitivity in detecting pulmonary gas exchange dysfunction in the SI-ALI animal model. As a widely used ^{129}Xe MR biomarker, RBC/TP has been employed to quantify changes in gas exchange function associated with lung diseases, such as COPD, IPF, and COVID-19 [29–32]. RBC/TP significantly decreased ($p = 0.035$) in the SII group, primarily due to increased septal wall thickness, as corroborated by histology. Furthermore, RBC/TP also demonstrated a strong correlation with FVC and MLD ($p < 0.01$), indicating its capacity to accurately reflect functional changes of the lungs caused by smoke exposure.

Compared to the sham group, the significantly higher T and d values were observed in the SII group ($p < 0.05$). These changes are probably attributed to alveolar wall thickening. Following smoke exposure, the mean septal wall thickness increased by approximately 17% compared to that in the sham group. Histology confirmed these structural changes, including neutrophil infiltration and edema [33,34]. The significant correlation between septal wall thickness measured by MR and by histology ($R^2 = 0.72$) further validated MR-based assessments. Additionally, SII rats exhibited a significant reduction in SVR, likely due to decreases lung volume and a consequent reduction in the respiratory membrane area available for gas exchange.

Hyperpolarized ^{129}Xe MRI has received regulatory approval for clinical use in China, the United States, and several European countries. Its utility has been extensively validated in respiratory diseases such as COPD, asthma, and IPF, where it has demonstrated high sensitivity to early functional impairment [35,36]. As a non-invasive modality, the technique requires only the inhalation of the hyperpolarized gas followed by a brief breath-hold, with key image acquisition possible within a single 10–15 s breath-hold, without sedation. This enables comprehensive three-dimensional visualization and quantification of pulmonary ventilation, gas exchange, and microstructure [37,38].

^{129}Xe MRI offers distinct and complementary advantages compared to CT. While CT remains the primary modality for identifying morphological abnormalities such as consolidation and severe edema, it lacks the ability to directly assess pulmonary function. ^{129}Xe MRI fills this gap by providing a direct, quantitative measure of gas exchange efficiency at the alveolar-capillary barrier through the RBC/TP ratio and by mapping ventilation defects. These functional capabilities are absent in conventional CT. Furthermore, the radiation-free safety profile of ^{129}Xe MRI is well-established even in pediatric populations [39,40], significantly facilitates repeated longitudinal monitoring, which is often limited in CT due to cumulative radiation risks.

In contrast to FOB, whose principal strengths are the direct visualization of airway mucosa and therapeutic intervention (e.g., clearance of obstructions), ^{129}Xe MR provides a rapid, non-invasive, and highly sensitive quantitative assessment of pulmonary gas exchange function. Beyond the whole-lung metrics reported in this study, the technique also enables regional functional mapping. Such regional analysis, successfully applied in other respiratory diseases, holds potential for guiding precision medicine and personalized treatment strategies in SI-ALI.

Regarding its clinical integration, ^{129}Xe MRI is best positioned as a complementary tool rather than a replacement for CT or FOB. An optimal clinical sequence may involve initial CT for structural diagnosis and FOB for acute airway management, followed by ^{129}Xe MRI for establishing a functional baseline and monitoring subsequent recovery. The primary barrier to widespread adoption is cost, as the need for gas hyperpolarization renders ^{129}Xe MRI more expensive than conventional MRI or CT. However, this cost must be evaluated against the unique functional insights it provides, which are unobtainable by other means. In summary, hyperpolarized ^{129}Xe MRI represents a valuable adjunct in the management of SI-ALI, offering critical functional information that complements existing structural and endoscopic modalities.

This study aimed to investigate the feasibility and potential of hyperpolarized ^{129}Xe MR for evaluating the impact of SI-ALI on pulmonary microstructure and gas exchange function. However, several limitations must be acknowledged. First, gas exchange assessment was performed globally using CSSR; future studies should incorporate regional dissolved-phase ^{129}Xe imaging to capture spatial heterogeneity [41,42]. Second, examinations were performed at 24 h post-injury, coinciding with the peak inflammatory response [43,44]; longitudinal imaging would better characterize disease progression. Third, the rat model used in this study does not fully replicate the complex pathophysiology of human smoke inhalation injuries. Modern fires involve more diverse and toxic materials [45,46], suggesting a need for more representative exposure models. Finally, although statistically significant differences in key parameters were observed between the SII and Sham groups, the sample size was relatively small ($n = 5$). Future studies with larger cohorts are warranted to further validate these findings.

5. Conclusion

In summary, hyperpolarized ^{129}Xe MR effectively evaluated changes in lung structure and function in an animal model of SI-ALI. Parameters such as RBC/TP and T could sensitively assess impairments in gas exchange function, while ventilation imaging effectively reflects regional ventilation deficits consistent with Micro-CT findings. The septal wall thickness measured via ^{129}Xe MR also correlates strongly with histology. These findings support the potential clinical application of hyperpolarized ^{129}Xe MR for assessing smoke-inhalation-induced lung injury.

Ethics statement

All animal experimental protocols were approved by the Institutional Review Board (APM25001A).

Funding

This work was supported by National Natural Science Foundation of China (82441015, T2522037, 82502586, 82441012 and 82272109), the Strategic Priority Research Program of the Chinese Academy of Sciences (XDC0170000 and XDB0540000), Scientific Instrument Developing Project of the Chinese Academy of Sciences (PTYQ2024TD0001), Key Research Program of Frontier Sciences, CAS (ZDBS-LY-JSC004), and Hubei Province Science and Technology Innovation Talent Program (2024DJA001).

Declaration of Competing Interest

The authors declare that they have no known competing financial interests or personal relationships that could have appeared to influence the work reported in this paper.

Acknowledgments

Not applicable

Data availability

The data that supports the findings of this study are available from the corresponding author upon reasonable request

References

[1] Guo B, Bai Y, Ma Y, Liu C, Wang S, Zhao R, et al. Preclinical and clinical studies of smoke-inhalation-induced acute lung injury: update on both pathogenesis and innovative therapy. Ther Adv Respir Dis 2019;13:1753466619847901. https://doi.org/10.1177/1753466619847901.

[2] Shirani KZ, Pruitt BA, Mason AD. The influence of inhalation injury and pneumonia on burn mortality. Ann Surg 1987;205:82–7. https://doi.org/10.1097/00000658-198701000-00015.

[3] Galeiras R, Seoane-Quiroga L, Pértega-Díaz S. Prevalence and prognostic impact of inhalation injury among burn patients: a systematic review and meta-analysis. J Trauma Acute Care Surg 2020;88:330–44. https://doi.org/10.1097/TA.0000000000002523.

[4] Taylor SL, Sen S, Greenhalgh DG, Lawless M, Curri T, Palmieri TL. A competing risk analysis for hospital length of stay in patients with burns. JAMA Surg 2015;150:450–6. https://doi.org/10.1001/jamasurg.2014.3490.

[5] Gattinoni L, Caironi P, Valenza F, Carlesso E. The role of CT-scan studies for the diagnosis and therapy of acute respiratory distress syndrome. Clin Chest Med 2006;27:559–70. https://doi.org/10.1016/j.ccm.2006.06.002.

[6] Peitzman AB, Shires GT, 3rd, Teixidor HS, Curreri PW, Shires GT. Smoke inhalation injury: evaluation of radiographic manifestations and pulmonary dysfunction. ; discussion 1238-1239 J Trauma 1989;29:1232–8. https://doi.org/10.1097/00005373-198909000-00008.

[7] Carr JA, Phillips BD, Bowling WM. The utility of bronchoscopy after inhalation injury complicated by pneumonia in burn patients: results from the National Burn

Repository. J Burn Care & Res Publ Am Burn Assoc 2009;30:967–74. https://doi.org/10.1097/BCR.0b013e3181bfb77b.
[8] Spano S, Hanna S, Li Z, Wood D, Cartotto R. Does bronchoscopic evaluation of inhalation injury severity predict outcome? J Burn Care & Res Publ Am Burn Assoc 2016;37:1–11. https://doi.org/10.1097/BCR.0000000000000320.
[9] Walker PF, Buehner MF, Wood LA, Boyer NL, Driscoll IR, Lundy JB, et al. Diagnosis and management of inhalation injury: An updated review. Crit Care 2015;19:351. https://doi.org/10.1186/s13054-015-1077-4.
[10] Davis CS, Janus SE, Mosier MJ, Carter SR, Gibbs JT, Ramirez L, et al. Inhalation injury severity and systemic immune perturbations in burned adults. Ann Surg 2013;257:1137–46. https://doi.org/10.1097/SLA.0b013e318275f424.
[11] Yang Y, Yue S, Shen L, Dong H, Li H, Zhao X, et al. Ultrasensitive ^{129}Xe magnetic resonance imaging: From clinical monitoring to molecular sensing. Adv Sci 2025; 12:e2413426. https://doi.org/10.1002/advs.202413426.
[12] Mummy DG, Coleman EM, Wang Z, Bier EA, Lu J, Driehuys B, et al. Regional gas exchange measured by ^{129}Xe magnetic resonance imaging before and after combination bronchodilators treatment in chronic obstructive pulmonary disease. J Magn Reson Imaging 2021;54:964–74. https://doi.org/10.1002/jmri.27662.
[13] Zhang M, Li H, Li H, Zhao X, Zhou Q, Rao Q, et al. Quantitative evaluation of lung injury caused by $PM_{2.5}$ using hyperpolarized gas magnetic resonance. Magn Reson Med 2020;84:569–78. https://doi.org/10.1002/mrm.28145.
[14] Garrison WJ, Qing K, He M, Zhao L, Tustison NJ, Patrie JT, et al. Lung volume dependence and repeatability of Hyperpolarized ^{129}Xe MRI gas uptake metrics in healthy volunteers and participants with COPD. Radio Cardiothorac Imaging 2023; 5:e220096. https://doi.org/10.1148/ryct.220096.
[15] Kieninger E, Munidasa S, Curdy M, Streibel C, Zanette B, Woods J, et al. Application of the defect distribution index to functional lung MRI of pediatric cystic fibrosis lung disease and controls. J Cyst Fibros 2025;S1569-1993(25): 00065–7. https://doi.org/10.1016/j.jcf.2025.02.015.
[16] Friedlander Y, Munidasa S, Thakar A, Ragunayakam N, Venegas C, Kjarsgaard M, et al. Phase-resolved functional lung (PREFUL) MRI to quantify ventilation: Feasibility and physiological relevance in severe asthma. Acad Radio 2024;31: 3416–26. https://doi.org/10.1016/j.acra.2024.01.039.
[17] Mercel AI, Gillis DC, Sun K, Dandurand BR, Weiss JM, Tsihlis ND, et al. A comparative study of a preclinical survival model of smoke inhalation injury in mice and rats. Am J PhysiolLung Cell Mol Physiol 2020;319:L471–80. https://doi.org/10.1152/ajplung.00241.2020.
[18] Li H, Li H, Fan L, Zhang M, Liu X, Zhao X, et al. Dynamic ventilation functional MRI of the lung with sub-millimeter spatial resolution and millisecond temporal resolution. 00498-0 Sci Bull 2025;S2095-9273(25). https://doi.org/10.1016/j.scib.2025.05.014.
[19] Zhang M, Li H, Li H, Zhao X, Liu X, Han Y, et al. Dynamic evaluation of acute lung injury using hyperpolarized 129 xe magnetic resonance. NMR Biomed 2024;37: e5078. https://doi.org/10.1002/nbm.5078.
[20] Chang YV. MOXE: A model of gas exchange for hyperpolarized ^{129}Xe magnetic resonance of the lung. Magn Reson Med 2013;69:884–90. https://doi.org/10.1002/mrm.24304.
[21] Li H, Zhang Z, Zhao X, Han Y, Sun X, Ye C, et al. Quantitative evaluation of pulmonary gas-exchange function using hyperpolarized ^{129}Xe CEST MRS and MRI. NMR Biomed 2018;31:e3961. https://doi.org/10.1002/nbm.3961.
[22] ITK-SNAP home n.d. ⟨https://www.itksnap.org/pmwiki/pmwiki.php⟩ (accessed June 3, 2025).
[23] Pua ZJ, Stonestreet BS, Cullen A, Shahsafaei A, Sadowska GB, Sunday ME. Histochemical analyses of altered fetal lung development following single vs multiple courses of antenatal steroids. Journal Histochemistry Cytochemistry Official Journal Histochemistry Society 2005;53:1469–79. https://doi.org/10.1369/jhc.5A6721.2005.
[24] Ruan W, Zhong J, Guan Y, Xia Y, Zhao X, Han Y, et al. Detection of smoke-induced pulmonary lesions by hyperpolarized 129 xe diffusion kurtosis imaging in rat models. Magn Reson Med 2017;78:1891–9. https://doi.org/10.1002/mrm.26566.
[25] Li H, Zhang Z, Zhao X, Sun X, Ye C, Zhou X. Quantitative evaluation of radiation-induced lung injury with hyperpolarized xenon magnetic resonance. Magn Reson Med 2016;76:408–16. https://doi.org/10.1002/mrm.25894.
[26] David P, Dunsford D, Lu J, Moochhala S. Animal models of smoke inhalation induced injuries. Front Biosci (Landmark Ed) 2009;14:4618–30. https://doi.org/10.2741/3554.
[27] Enkhbaatar P, Pruitt BA, Suman O, Mlcak R, Wolf SE, Sakurai H, et al. Pathophysiology, research challenges, and clinical management of smoke inhalation injury. Lancet (Lond Engl) 2016;388:1437–46. https://doi.org/10.1016/S0140-6736(16)31458-1.
[28] Wolfe AG, Stillwell PC, Veress LA. Significant airway obstruction by carbonaceous fibrin casts in a child with smoke inhalation injury. Am J Respir Crit Care Med 2024;209:1392–3. https://doi.org/10.1164/rccm.202212-2289IM.
[29] Li H, Zhao X, Wang Y, Lou X, Chen S, Deng H, et al. Damaged lung gas exchange function of discharged COVID-19 patients detected by hyperpolarized ^{129}Xe MRI. Sci Adv 2021;7:eabc8180. https://doi.org/10.1126/sciadv.abc8180.
[30] Hahn AD, Carey KJ, Barton GP, Torres LA, Kammerman J, Cadman RV, et al. Hyperpolarized^{129} xe MR spectroscopy in the lung shows 1-year reduced function in idiopathic pulmonary fibrosis. Radiology 2022;305:688–96. https://doi.org/10.1148/radiol.211433.
[31] Shen L, Li H, Fang Y, Luo M, Li Y, Zhou Q, et al. Hyperpolarized ^{129}Xe diffusion-weighted MRI of the lung with 3D golden-angle radial sampling and keyhole reconstruction. Med Phys 2025. https://doi.org/10.1002/mp.17719.
[32] Fang Y, Li H, Shen L, Zhang M, Luo M, Li H, et al. Rapid pulmonary ^{129}Xe ventilation MRI of discharged COVID-19 patients with zigzag sampling. Magn Reson Med 2024;92:956–66. https://doi.org/10.1002/mrm.30120.
[33] Tsikis ST, Fligor SC, Hirsch TI, Pan A, Yu LJ, Kishikawa H, et al. Lipopolysaccharide-induced murine lung injury results in long-term pulmonary changes and downregulation of angiogenic pathways. Sci Rep 2022;12:10245. https://doi.org/10.1038/s41598-022-14618-8.
[34] Wang JM, Robertson SH, Wang Z, He M, Virgincar RS, Schrank GM, et al. Using hyperpolarized^{129} xe MRI to quantify regional gas transfer in idiopathic pulmonary fibrosis. Thorax 2018;73:21–8. https://doi.org/10.1136/thoraxjnl-2017-210070.
[35] Li H, Li H, Zhang M, Fang Y, Shen L, Liu X, et al. Advancements and applications of hyperpolarized xenon MRI for chronic obstructive pulmonary disease assessment in China. Br J Radio 2025:tqaf119. https://doi.org/10.1093/bjr/tqaf119.
[36] Li H, Li H, Zhang M, Huang C, Zhou X. Direct imaging of pulmonary gas exchange with hyperpolarized xenon MRI. Innov (Camb) 2024;5:100720. https://doi.org/10.1016/j.xinn.2024.100720.
[37] Zhang M, Li H, Xiao Y, Li H, Liu X, Zhao X, et al. Assessment of Global and Regional Lung Compliance in Pulmonary Fibrosis With Hyperpolarized Gas. J Magn Reson Imaging 2025;61:1404–15. https://doi.org/10.1002/jmri.29497.
[38] Rao Q, Li H, Zhou Q, Zhang M, Zhao X, Shi L, et al. Assessment of pulmonary physiological changes caused by aging, cigarette smoking, and COPD with hyperpolarized ^{129}Xe magnetic resonance. Eur Radio 2024;34:7450–9. https://doi.org/10.1007/s00330-024-10800-w.
[39] Driehuys B, Martinez-Jimenez S, Cleveland ZI, Metz GM, Beaver DM, Nouls JC, et al. Chronic obstructive pulmonary disease: Safety and tolerability of hyperpolarized ^{129}Xe MR imaging in healthy volunteers and patients. Radiology 2012;262:279–89. https://doi.org/10.1148/radiol.11102172.
[40] Walkup LL, Thomen RP, Akinyi TG, Watters E, Ruppert K, Clancy JP, et al. Feasibility, tolerability and safety of pediatric hyperpolarized ^{129}Xe magnetic resonance imaging in healthy volunteers and children with cystic fibrosis. Pedia Radio 2016;46:1651–62. https://doi.org/10.1007/s00247-016-3672-1.
[41] Zanette B, Santyr G. Accelerated interleaved spiral-IDEAL imaging of hyperpolarized^{129} xe for parametric gas exchange mapping in humans. Magn Reson Med 2019;82:1113–9. https://doi.org/10.1002/mrm.27765.
[42] Qing K, Ruppert K, Jiang Y, Mata JF, Miller GW, Shim YM, et al. Regional mapping of gas uptake by blood and tissue in the human lung using hyperpolarized xenon-129 MRI. J Magn Reson Imaging 2014;39:346–59. https://doi.org/10.1002/jmri.24181.
[43] Zhu F, Qiu X, Wang J, Jin Y, Sun Y, Lv T, et al. A rat model of smoke inhalation injury. Inhal Toxicol 2012;24:356–64. https://doi.org/10.3109/08958378.2012.673179.
[44] Guo H, Yang R, He J, Chen K, Yang W, Liu J, et al. Edaravone combined with dexamethasone exhibits synergic effects on attenuating smoke-induced inhalation lung injury in rats. Biomed & Pharmacother 2021;141:111894. https://doi.org/10.1016/j.biopha.2021.111894.
[45] Prien T, Traber DL. Toxic smoke compounds and inhalation injury—a review. Burns 1988;14:451–60. https://doi.org/10.1016/S0305-4179(88)80005-6.
[46] Reczyńska K, Tharkar P, Kim SY, Wang Y, Pamuła E, Chan H-K, et al. Animal models of smoke inhalation injury and related acute and chronic lung diseases. Adv Drug Deliv Rev 2018;123:107–34. https://doi.org/10.1016/j.addr.2017.10.005.